Mechanical Systems and Signal Processing 149 (2021) 107216

Contents lists available at ScienceDirect

Mechanical Systems and Signal Processing

journal homepage: www.elsevier.com/locate/ymssp

Uniformly optimal multi-sensor design in pipe networks for transient-based leakage localization

Xun Wang

Key Laboratory on Reliability and Environmental Engineering Technology, School of Reliability and Systems Engineering, Beihang University, Xueyuan Road No. 37, Haidian District, Beijing 100083, China

ARTICLE INFO

Article history:
Received 2 March 2020
Received in revised form 24 July 2020
Accepted 10 August 2020

Keywords:
Sensor design
Transient wave
Pipe network
Fisher information
Cramér–Rao lower bound
Quasi-Monte-Carlo simulation

ABSTRACT

The design of sensor placement in water supply pipe networks for the purpose of transient-based leakage localization is investigated. Each sensor is placed at where the Fisher information of measurement concerning leaks is maximized; equivalently, the Cramér–Rao lower bound (CRLB) representing the lower limit of leak localization error is minimized. An explicit algorithm for computing the CRLB with respect to leak parameters in a general pipe network is developed. The presence of leak is considered as stochastic and modeled in a probabilistic framework by assuming that the leak location follows a probabilistic distribution with a support on the whole network. The optimal distribution of the sensors is then computed via a quasi-Monte-Carlo simulation, where the expectation of the CRLB of leak localization error is minimized. The proposed sensor placement methodology is optimal uniformly over all the leak localization methods, all the potential sensor locations and all the situations of leaks. Four examples from a simple single-pipe system to a complex pipe network are presented to illustrate the proposed methodology.

1. Introduction

Leakage is a serious problem persisting in water supply systems; the water lost worldwide amounts to USD 39 billion per year according to a recent report [1]. Active transient wave-based methodology is a promising general approach for estimating leaks and other defects [2–10]. This approach actively introduces transient waves in the fluid, measures pressure response at specified locations, and analyzes the measured signals to identify leaks in a pipe system. This approach has been deeply investigated in the past two decades and successfully used in pipe networks [11–19] and several field tests such as [20–26].

The accuracy of the transient-based leakage detection largely depends on the quality and quantity of measurements, especially in real environments where the measured signals are often contaminated by noise. Currently, urban pipe networks, as well as other large and complex civil infrastructures, always install a large number of sensors to monitor their health condition [27–30]. However, as the measurements at different locations in a pipe network are not equally effective and bring different quantity of information regarding leaks [31], the design of the sensors is important. It is suggested in [3] that measurements should be made in a location being sensitive to the desired parameters. The optimal design of measurement location has been studied in [31–34] where the criterion is to minimize the leak localization error of the inverse transient analysis (ITA) method [3,35] or maximizing the sensitivity of the pressure measurement model with respect to

E-mail address: xunwang@buaa.edu.cn

https://doi.org/10.1016/j.ymssp.2020.107216
0888-3270/

Nomenclature

q	discharge oscillation
h	pressure head oscillation
x^U (x^D)	upstream (downstream) end of pipe
x^L	leak location
s^L	leak size
Q_0^L, H_0^L	steady-state discharge and head of leak
Q_0	steady-state discharge of main pipe
$\mathcal{X}$	coordinate system of a pipe network
x^S	sensor coordinate
x_p	coordinate in p-th pipe
a	wave speed
A	internal area of pipe
l	pipe length
d	internal pipe diameter
M	number of sensors
J	number of frequencies
N	number of nodes in a network
P	number of pipes in a network
CRLB	Cramér–Rao lower bound
FI	Fisher information
FIM	Fisher information matrix
ML	maximum likelihood
MOC	method of characteristic
MSE	mean square error
PDF	probability density function
QMC	quasi Monte-Carlo

unknown parameters. However, in these works, only very simple cases can be considered where the sensors, as well as leaks, can only be located at the junctions of network. For example, in the network in Fig. 1 in [31] which has eleven pipes with in total 11×747 m long, only six nodes can be potential locations of sensor and leak. This is not realistic because leaks may occur anywhere and, general speaking, the junctions are not the optimal measurement locations. The more practical cases where a sensor and a leak can be located at anywhere in a network cannot be solved by [31–34], because these methods involve either a full enumeration or an optimization solution of sensor locations which needs a large amount of numerical simulation (wave propagation simulation in the time domain). Therefore, the present paper aims at proposing a novel sensor design methodology by which sensors can be freely put anywhere in a pipe network and all the possible situations of leak are considered.

Fisher information (FI) is a measure of amount of information that a measurement carries about an unknown parameter. Cramér–Rao lower bound (CRLB) provides a tool to assess how accurate this unknown parameter can be estimated given this measurement, more exactly the best achievable performance of the parameter estimation or the minimum attainable error. This theoretical limit of parameter estimation is asymptotically reachable by the maximum likelihood (ML) and the multiple signal classification (MUSIC) methods [36], which have been applied in the pipeline leakage detection problem [37–40]. The computation of CRLB of transient measurement concerning leakage and blockage in a single pipe has been reported in [37,41,42] and used to evaluate the performance of leakage/blockage detection methods. The FI theory and CRLB are also powerful tools to investigate the performance of sensor arrays with arbitrary distribution for free-field source estimation [43–48]. In this paper, an algorithm for computing the FI and CRLB in a general pipe network is developed; furthermore, the sensor displacement is optimized by maximizing the FI of measurement or minimizing the CRLB among all the possible combinations of sensors.

In practice, the appearance of leak is stochastic; it can occur anywhere in a network with any leak size in a reasonable interval. This must be considered in the sensor design but the exhaustion of all possible cases of leakage would not be applicable [31]. Given a probabilistic distribution of the leak parameters, the Monte-Carlo method is able to realize the stochastic modeling by repeating random sampling of leak parameters and computing the corresponding CRLBs. The computation and convergence of the stochastic simulation can be accelerated with less samples using pseudo-random sequences, known as the quasi-Monte-Carlo (QMC) methods [49,50]. In this paper, Sobol' sequence [51], which is a specific QMC method with low-discrepancy, is employed to simulate the appearance of a leak in a pipe network, by which the expectation of CRLB is computed and minimized to design the sensor array.

The proposed sensor design approach is called "uniformly" optimal for the following three reasons: (i) the optimal measurement sites are selected from all the possible locations in a pipe network; (ii) the sensor design globally considers all the

possible situations of leakage (in a probabilistic framework); (iii) the design is not dependent on any specific leak detection method but valid for all the methods in terms of maximum measurement information.

The next section illustrates the general methodology of sensor placement design in a pipeline system. Specific computation procedure and results for single-pipe systems and networks are given in Sections 3 and Section 4, respectively. Finally, conclusions are drawn in Section 5.

2. General methodology

2.1. A brief review of FI theory and CRLB

Let ξ represent a random variable with probability density function (PDF) $f(x|\theta)$, where θ is the parameter of the probabilistic distribution. FI is a measure of information of θ; it quantifies the information of a sample that can provide about the parameter θ. FI is defined by

$$I(\theta) = -\mathbb{E}\left(\frac{d^2 \log f(x|\theta)}{d\theta^2}\right) = -\int \frac{d^2 \log f(x|\theta)}{d\theta^2} f(x|\theta) dx. \tag{1}$$

It decides the lowest possible variance, or mean square error (MSE), of the estimation of θ, among all the parameter estimation methods, by

$$\mathrm{Var}\left(\hat{\theta}\right) \geqslant \left(\frac{d\mathbb{E}\left(\hat{\theta}\right)}{d\theta}\right)^2 \frac{1}{TI(\theta)}, \tag{2}$$

where $\hat{\theta}$ is an estimator of θ and T is the sample size. If $\hat{\theta}$ is unbiased, i.e., $\mathbb{E}\left(\hat{\theta}\right) = \theta$, then

$$\mathrm{Var}\left(\hat{\theta}\right) \geqslant \frac{1}{TI(\theta)}. \tag{3}$$

The right hand side of Eq. (3) is known as the CRLB. For the case of multiple unknown parameters, denoted as $\Theta = (\theta_1, \ldots, \theta_N)$, the sample information is described by the Fisher information matrix (FIM):

$$\mathbf{I}(\Theta) = -\mathbb{E}\left(\frac{d^2 \log f(x|\Theta)}{d\Theta^2}\right) = -\left(\int \frac{d^2 \log f(x|\Theta)}{d\theta_{n_1} d\theta_{n_2}} f(x|\Theta) dx\right)_{n_1=1, n_2=1}^{N,N}. \tag{4}$$

Similarly, the CRLB for the covariance matrix estimate is obtained from the FIM:

$$\mathrm{Cov}\left(\hat{\Theta}\right) \geqslant (T\mathbf{I}(\Theta))^{-1}. \tag{5}$$

Note that the CRLB is asymptotically attainable by the ML estimation [37]: the MSE or the covariance matrix of the estimate of θ or Θ using ML achieves the CRLB when the sample size tends to infinity.

2.2. Computation of FI and CRLB of pressure measurement in a pipe system

Let $\mathcal{X}$ denote the coordinate system of a general pipe network. Consider a leak in the system whose location is $x^L \in \mathcal{X}$ and the corresponding leak size (effective leak orifice area) is s^L. The sensors are placed at $\{x_m^S : m = 1, \ldots, M\} \subset \mathcal{X}$, where M is the number of sensors.

After sending an active transient wave, pressure heads at the M sensors are measured. From each sensor, J data are collected; thus the data for leakage detection are $\mathbf{h} = \mathrm{vec}\{h_{mj}, m = 1, \ldots M, j = 1, \ldots, J\}$. Let $\mathbf{h}^{model}(x^L, s^L) = \mathrm{vec}\left\{h_{mj}^{model}(x^L, s^L), m = 1, \ldots M, j = 1, \ldots, J\right\}$ denote the physical model of $\mathbf{h}$, thus $\mathbf{h}$ has the theoretical expression

$$\mathbf{h} = \mathbf{h}^{model}(x^L, s^L) + \mathbf{n}. \tag{6}$$

Here, $\mathbf{n} = \mathrm{vec}\{n_{mj}, m = 1, \ldots M, j = 1, \ldots, J\}$ is an additive error term, where n_{mj}'s are independent and identically distributed and follow Gaussian distribution with zero-mean and equal variance σ^2 (i.e., independent Gaussian white noise). The Gaussian assumption has been justified to be reasonable via an experimental study of noise in different pipe systems in [52]. In the case that $\mathbf{n}$ is nonwhite and/or correlated (with a general covariance matrix), a noise whitening scheme in [9] can be applied such that the assumption still holds. It is also emphasized that, in practice, the mismatch between the data $\mathbf{h}$ and the model $\mathbf{h}^{model}(x^L, s^L)$ involves not only random error but also (non-random) modeling error [53,54]. The latter is not considered in the present paper. However, as is shown in [55], if transient tests are routinely practiced, the modeling error of a

pipe system can be identified before any major defect exists; then, when a leak appears, the modeling error in transient signals for leakage detection can be canceled such that Eq. (6) holds.

On the basis of the model in Eq. (6), the log-likelihood function of $\mathbf{h}$ is

$$\log L(x^L, s^L|\mathbf{h}) = \sum_{m=1}^{M}\sum_{j=1}^{J} \log L(x^L, s^L|h_{mj}), \tag{7}$$

in which

$$\begin{aligned}\log L(x^L, s^L|h_{mj}) &= \log f(h_{mj}|x^L, s^L) = -\log(\pi\sigma^2) - \frac{1}{\sigma^2}\left\|h_{mj} - h_{mj}^{model}\right\|^2 \\ &= -\log(\pi\sigma^2) - \frac{1}{\sigma^2}\left[h_{mj}^c h_{mj} - h_{mj}^c h_{mj}^{model} - \left(h_{mj}^{model}\right)^c h_{mj} + \left(h_{mj}^{model}\right)^c h_{mj}^{model}\right],\end{aligned} \tag{8}$$

where the superscript c represents the complex conjugate operation.[1] For any $\theta_1 \in \{x^L, s^L\}$ and $\theta_2 \in \{x^L, s^L\}$,

$$\begin{aligned}\sigma^2\frac{\partial^2 \log L(x^L, s^L|h_{mj})}{\partial\theta_1\partial\theta_2} &= h_{mj}^c\frac{\partial^2 h_{mj}^{model}}{\partial\theta_1\partial\theta_2} + \left(\frac{\partial^2 h_{mj}^{model}}{\partial\theta_1\partial\theta_2}\right)^c h_{mj} - \left(h_{mj}^{model}\right)^c\frac{\partial^2 h_{mj}^{model}}{\partial\theta_1\partial\theta_2} - \left(\frac{\partial^2 h_{mj}^{model}}{\partial\theta_1\partial\theta_2}\right)^c h_{mj}^{model} - \left(\frac{\partial h_{mj}^{model}}{\partial\theta_1}\right)^c\frac{\partial h_{mj}^{model}}{\partial\theta_2} \\ &\quad - \left(\frac{\partial h_{mj}^{model}}{\partial\theta_2}\right)^c\frac{\partial h_{mj}^{model}}{\partial\theta_1}.\end{aligned} \tag{9}$$

Taking mathematical expectation on both sides of Eq. (9), we obtain

$$\mathbb{E}\left(\frac{\partial^2 \log L(x^L, s^L|h_{mj})}{\partial\theta_1\partial\theta_2}\right) = -\frac{1}{\sigma^2}\left[\left(\frac{\partial h_{mj}^{model}}{\partial\theta_1}\right)^c\frac{\partial h_{mj}^{model}}{\partial\theta_2} + \left(\frac{\partial h_{mj}^{model}}{\partial\theta_2}\right)^c\frac{\partial h_{mj}^{model}}{\partial\theta_1}\right], \tag{10}$$

thus

$$\mathbb{E}\left(\frac{\partial^2 \log L(x^L, s^L|\mathbf{h})}{\partial\theta_1\partial\theta_2}\right) = -\frac{1}{\sigma^2}\left[\left(\frac{\partial \mathbf{h}^{model}}{\partial\theta_1}\right)^H\frac{\partial \mathbf{h}^{model}}{\partial\theta_2} + \left(\frac{\partial \mathbf{h}^{model}}{\partial\theta_2}\right)^H\frac{\partial \mathbf{h}^{model}}{\partial\theta_1}\right], \tag{11}$$

in which the superscript "H" stands for the conjugate transpose operation of a vector. Eqs. (10) and (11) imply that in practice only the first order derivative is needed for computing FI and CRLB.

The FIM has the expression

$$\mathbf{I}(x^L, s^L) = \begin{pmatrix} I_{xx} & I_{xs} \\ I_{sx} & I_{ss} \end{pmatrix}, \tag{12}$$

in which

$$I_{xx} = \frac{2}{\sigma^2}\left(\frac{\partial \mathbf{h}^{model}}{\partial x^L}\right)^H\frac{\partial \mathbf{h}^{model}}{\partial x^L}, \tag{13}$$

$$I_{xs} = \frac{1}{\sigma^2}\left[\left(\frac{\partial \mathbf{h}^{model}}{\partial x^L}\right)^H\frac{\partial \mathbf{h}^{model}}{\partial s^L} + \left(\frac{\partial \mathbf{h}^{model}}{\partial s^L}\right)^H\frac{\partial \mathbf{h}^{model}}{\partial x^L}\right], \tag{14}$$

$$I_{sx} = \frac{1}{\sigma^2}\left[\left(\frac{\partial \mathbf{h}^{model}}{\partial s^L}\right)^H\frac{\partial \mathbf{h}^{model}}{\partial x^L} + \left(\frac{\partial \mathbf{h}^{model}}{\partial x^L}\right)^H\frac{\partial \mathbf{h}^{model}}{\partial s^L}\right], \tag{15}$$

$$I_{ss} = \frac{2}{\sigma^2}\left(\frac{\partial \mathbf{h}^{model}}{\partial s^L}\right)^H\frac{\partial \mathbf{h}^{model}}{\partial s^L}. \tag{16}$$

Then, the CRLB of x^L, s^L given each $\mathbf{h}$ (the sample size $T = 1$) is

$$\mathrm{CRLB}(x^L, s^L) = \mathbf{I}^{-1}(x^L, s^L). \tag{17}$$

[1] Without loss of generality, the pressure heads are assumed as complex-valued. Actually, the frequency-domain transient-wave model is considered in each example in this paper where the data are all complex-valued; however, the FI and CRLB can be similarly computed with the time-domain model as in [41,42].

Since, in practice, the main concern is the leak localization, in this paper the optimal locations of the sensors are decided by minimizing the expected MSE of the estimate of x^L, i.e., the $(1,1)$-element of Eq. (17).

2.3. Optimal sensor placement

In practice, the appearance of a leak is stochastic and it can be located at anywhere in a pipe network. The leak size is also random within a range. In order to consider all the possibilities of leak in the sensor placement design, x^L and s^L are assumed as random variables with PDFs $f_x(x^L)$ and $f_s(s^L)$, respectively. The PDF $f_x(x^L)$ of x^L has the support on $\mathcal{X}$, i.e., the leak may appear anywhere in the system. If no prior information about x^L is available, according to the principle of maximum entropy [56], x^L is assumed to follow the uniform distribution with support $\mathcal{X}$, denoted by $\mathrm{U}(\mathcal{X})$. In other cases where prior information is available, for example some sections of a pipe network are more aging and thus more probably have a leak, other distributions can be assumed. The leak size s^L is non-negative and in practice within an interval, denoted by $s^L \in [0, s^L_{\max}]$, where $s^L_{\max}$ is the upper bound of leak size. Again, in the case of no prior information, according to the principle of maximum entropy, s^L could be assumed to follow the uniform distribution with support $[0, s^L_{\max}]$, denoted by $\mathrm{U}([0, s^L_{\max}])$.

Stochastic simulation is employed to mimic the randomness of the both leak parameters. Quasi-Monte-Carlo (QMC) samples, realized by the Sobol' sequences [51] which are an example of quasi-random low-discrepancy sequences, are taken from f_x and f_s. More specifically, for $k \in \{1, \ldots, K\}$, two groups of QMC samples $x^L_{(k)} \sim f_x$ and $s^L_{(k)} \sim f_s$ are generated. The expectation of CRLB with respect to random x^L and s^L, denoted by $\mathbb{E}(\mathrm{CRLB})$, is estimated by the average of the K CRLBs corresponding to the K leak parameters.

Then, the optimal location of the first sensor, denoted by $\widehat{x^S_1}$, is decided by minimizing $\mathbb{E}(\mathrm{CRLB}(x^S))$, i.e., the expectation of minimum MSE of leak localization. If M $(M > 1)$ sensors are placed in the system, the additional gain of FI of measurement and the sensor ambiguity are considered simultaneously. The additional gain approach for deciding the second sensor means that, when two sensors are available, they are set at $\widehat{x^S_1}$ and a location which minimizes $\mathbb{E}\left(\mathrm{CRLB}\left(\widehat{x^S_1}, x^S\right)\right)$ with x^S. This is equivalent to optimizing the two sensors simultaneously because the noise is assumed to be independent at different places in the system and the CRLB is additive; this issue is also illustrated via a numerically example in Section 3.3. The sensor ambiguity means that when two sensors are overly close to each other, the measurements received from the both sensors are linearly dependent. To avoid this problem, it requires that the distance between two sensors is not lower than $\lambda_{\min}/2$ [43], where $\lambda_{\min}$ is the minimum wavelength of probing wave. Therefore, given $m-1$ sensors with locations $\widehat{x^S_i}, i = 1, \ldots, m-1$, the location of the m-th sensor is selected from the region in which every point is $\lambda_{\min}/2$ apart from the previous $m-1$ sensors, i.e.

$$\Omega_m = \mathcal{X} \cap \left(\cup_{i=1}^{m-1} \overline{B\left(\widehat{x^S_i}, \lambda_{\min}/2\right)} \right), \tag{18}$$

where $B(c, r)$ stands for a neighborhood set of c with radius r and $\overline{B}$ represents the complementary set of B. The specific steps of the proposed optimal design of sensor placement are given in Algorithm 1.

In the following two sections, a single pipe system (the typical reservoir-pipe-valve system) and pipe networks are respectively considered. The algorithm for the CRLB computation (Line 5 and 12 in Algorithm 1) in each example is explicitly given.

Algorithm 1 Uniformly optimal multi-sensor placement strategy

1: Let $m = 1$.
2: **for** $k = 1, \ldots, K$ **do**
3: Draw a QMC sample $x^L_{(k)} \sim f_x$;
4: Draw a QMC sample $s^L_{(k)} \sim f_s$;
5: Compute $\mathrm{CRLB}\left(x^L_{(k)}, s^L_{(k)} | x^S\right)$ for $x^S \in \mathcal{X}$;
6: **end for**
7: Decide the location of first sensor x_1 by

$$\widehat{x^S_1} = \arg\min_{x^S \in \mathcal{X}} \frac{1}{K} \sum_{k=1}^{K} \mathrm{CRLB}\left(x^L_{(k)}, s^L_{(k)} | x^S\right). \tag{19}$$

8: **for** $m = 2, \ldots, M$ **do**
9: **for** $k = 1, \ldots, K$ **do**

(*continued on next page*)

(*continued*)

Algorithm 1 Uniformly optimal multi-sensor placement strategy

10: Draw a QMC sample $x^L_{(km)} \sim f_x$;
11: Draw a QMC sample $s^L_{(km)} \sim f_s$;
12: Compute CRLB$\left(x^L_{(km)}, s^L_{(km)} | \widehat{x^S_1}, \ldots, \widehat{x^S_{m-1}}, x^S\right)$ for $x^S \in \Omega_m$;
13: **end for**
14: Decide the location of the m-th sensor by

$$\widehat{x^S_m} = \arg\min_{x^S \in \Omega_m} \frac{1}{K} \sum_{k=1}^{K} \mathrm{CRLB}\left(x^L_{(km)}, s^L_{(km)} | \widehat{x^S_1}, \ldots, \widehat{x^S_{m-1}}, x^S\right). \tag{20}$$

15: **end for**

3. Single-pipe system

3.1. Physical model

A typical reservoir-pipe-valve system is considered and illustrated by Fig. 1. In this case, $\mathcal{X} = \{x : x \in [0, l]\}$ and l is the length of the pipe.

The oscillations of discharge (volume rate of water flow) and pressure head in the frequency domain (more exactly, the frequency response function [57]) due to a fluid transient are represented by q and h. Given the discharge $q(x^U)$ and head $h(x^U)$ at the upstream node x^U, q and h at a sensor location x^S_m can be computed by the transfer matrix method [58,9]:

$$\begin{pmatrix} q(x^S_m) \\ h(x^S_m) \end{pmatrix} = \mathbf{M}^{NL}(x^S_m - x^L) \begin{pmatrix} 1 & -\frac{Q^L_0}{2(H^L_0 - z^L)} \\ 0 & 1 \end{pmatrix} \mathbf{M}^{NL}(x^L - x^U) \begin{pmatrix} q(x^U) \\ h(x^U) \end{pmatrix} = \left(\mathbf{M}^{NL}(x^S_m - x^U) + s^L \mathbf{M}^{SL}(x^L; x^U, x^S_m)\right) \begin{pmatrix} q(x^U) \\ h(x^U) \end{pmatrix}, \tag{21}$$

if $x^S_m > x^L$; and

$$\begin{pmatrix} q(x^S_m) \\ h(x^S_m) \end{pmatrix} = \mathbf{M}^{NL}(x^S_m - x^U) \begin{pmatrix} q(x^U) \\ h(x^U) \end{pmatrix}, \tag{22}$$

if $x^S_m < x^L$. Here, the effective leak size $s^L = \frac{Q^L_0}{\sqrt{2g(H^L_0 - z^L)}}$, where z^L is the elevation of the pipe at the leak, Q^L_0 is the steady-state outflow from the leak and H^L_0 is the steady-state pressure head at the leak,

$$\mathbf{M}^{NL}(x) = \begin{pmatrix} \cosh(\mu x) & -\frac{1}{Z}\sinh(\mu x) \\ -Z\sinh(\mu x) & \cosh(\mu x) \end{pmatrix} \tag{23}$$

is the field matrix,

$$\mathbf{M}^{SL}(x^L; x^U, x^D) = \sqrt{\frac{g}{2\left(H^L_0 - z^L\right)}} \begin{pmatrix} Z\sinh(\mu(x^L - x^U))\cosh(\mu(x^D - x^L)) & -\cosh(\mu(x^L - x^U))\cosh(\mu(x^D - x^L)) \\ -Z^2\sinh(\mu(x^L - x^U))\sinh(\mu(x^D - x^L)) & Z\cosh(\mu(x^L - x^U))\sinh(\mu(x^D - x^L)) \end{pmatrix}, \tag{24}$$

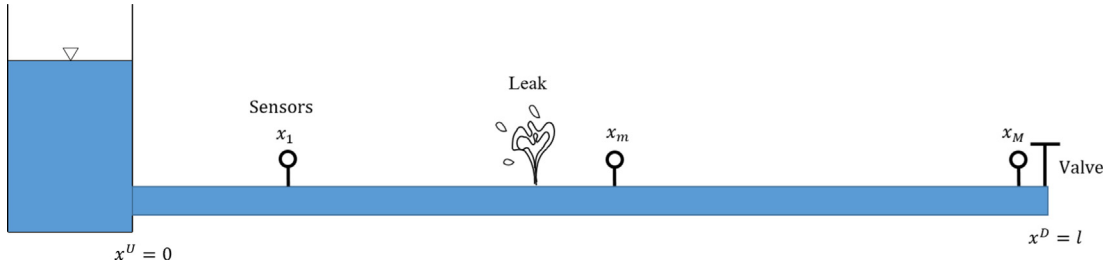

Fig. 1. Reservoir-pipe-valve system with multiple sensors.

$Z(\omega) = \mu(\omega)a^2/(\mathrm{i}\omega gA)$ is the characteristic impedance, $\mu(\omega) = a^{-1}\sqrt{-\omega^2 + \mathrm{i}gA\omega R}$ is the propagation function, a is the wave speed, ω is the angular frequency, A is the area of pipeline, and R is the frictional resistance term being $R = (f_{DW}Q_0)/\left(gdA^2\right)$ for turbulent flows, d is the pipe diameter and Q_0 is the steady-state discharge. Note that the transfer matrix method linearizes the steady friction and orifice equations [58,59]. The error due to this linearization is significant only if the perturbation of transient is more than 25% of the steady-state condition [60]. For leak detection, it is always the case that a much smaller wave is sent, thus the linearization error can be neglected.

In the reservoir-pipe-valve system, boundary conditions $h(x^U) = 0$ (x^U is connected to a reservoir) and $q(x^D) = 1$ (the transient wave is sent by the valve at x^D by an impulse-type perturbation of flow) can be reasonably assumed. As a result, the discharge at the upstream boundary is

$$q(x^U) = \frac{1}{\cosh(\mu x^D) + s^L k^L Z \sinh(\mu x^L)\cosh(\mu(x^D - x^L))}, \tag{25}$$

where $k^L \triangleq \sqrt{\frac{g}{2\left(H_0^L - z^L\right)}}$. Thus, the pressure head at the sensor x_m^S reads

$$h(x_m^S) = -Z\frac{\sinh(\mu x_m^S) + s^L k^L Z \sinh(\mu x^L)\sinh\left(\mu(x_m^S - x^L)\right)}{\cosh(\mu x^D) + s^L k^L Z \sinh(\mu x^L)\cosh(\mu(x^D - x^L))}, \tag{26}$$

if $x_m^S > x^L$; and

$$h(x_m^S) = -Z\frac{\sinh(\mu x_m^S)}{\cosh(\mu x^D) + s^L k^L Z \sinh(\mu x^L)\cosh(\mu(x^D - x^L))}, \tag{27}$$

if $x_m^S \leqslant x^L$.

3.2. CRLB computation

Let $Z_j \triangleq Z(\omega_j), \mu_j \triangleq \mu(\omega_j)$,

$$f_1 \triangleq \cosh\left(\mu_j x^D\right) + s^L k^L Z_j \sinh\left(\mu_j x^L\right)\cosh\left(\mu_j(x^D - x^L)\right) \tag{28}$$

and

$$f_2 \triangleq \begin{cases} \sinh\left(\mu_j x_m^S\right), \text{if } x_m^S \leqslant x^{L_n} \\ \sinh\left(\mu_j x_m^S\right) + s^L k^L Z_j \sinh\left(\mu_j x^L\right)\cosh\left(\mu_j(x_m^S - x^L)\right), \text{if } x_m^S > x^{L_n} \end{cases}. \tag{29}$$

The computation of FI and CRLB needs the first derivative:

$$\left(h_{mj}^{model}\right)' = -Z_j\frac{f_2' f_1 - f_1' f_2}{f_1^2}. \tag{30}$$

By Eqs. (28) and (29),

$$\frac{\partial f_1}{\partial x^L} = s^L k^L Z_j \mu_j\left(\cosh\left(\mu_j x^L\right)\cosh\left(\mu_j(x^D - x^L)\right) - \sinh\left(\mu_j x^L\right)\sinh\left(\mu_j(x^D - x^L)\right)\right) = s^L k^L Z_j \mu_j \cosh\left(\mu_j(2x^L - x^D)\right); \tag{31}$$

$$\frac{\partial f_1}{\partial s^L} = k^L Z_j \sinh\left(\mu_j x^L\right)\cosh\left(\mu_j(x^D - x^L)\right); \tag{32}$$

$$\frac{\partial f_2}{\partial x^L} = \begin{cases} 0, \text{ if } x_m^S \leqslant x^L \\ s^L k^L Z_j \mu_j \sinh\left(\mu_j(2x^L - x_m^S)\right), \text{ if } x_m^S > x^L \end{cases}; \tag{33}$$

and

$$\frac{\partial f_2}{\partial s^L} = \begin{cases} 0, \text{ if } x_m \leqslant x^L \\ k^L Z_j \sinh\left(\mu_j x^L\right)\sinh\left(\mu_j(x_m^S - x^L)\right), \text{ if } x_m^S > x^L \end{cases}. \tag{34}$$

Then,

$$\frac{\partial h_{mj}^{model}}{\partial x^L} = \begin{cases} Z_j\frac{f_2}{f_1^2}\frac{\partial f_1}{\partial x^L}, \text{ if } x_m^S \leqslant x^L \\ -Z_j\left(\frac{1}{f_1}\frac{\partial f_2}{\partial x^L} - \frac{f_2}{f_1^2}\frac{\partial f_1}{\partial x^L}\right), \text{ if } x_m^S > x^L \end{cases} \tag{35}$$

and

$$\frac{\partial h_{mj}^{model}}{\partial s^L} = \begin{cases} Z_j \frac{f_2}{f_1^2} \frac{\partial f_1}{\partial s^L}, & \text{if } x_m^S \leqslant x^L \\ -Z_j \left(\frac{1}{f_1} \frac{\partial f_2}{\partial s^L} - \frac{f_2}{f_1^2} \frac{\partial f_1}{\partial s^L} \right), & \text{if } x_m^S > x^L \end{cases}. \tag{36}$$

With the above two equations, the CRLB for any leak and sensor locations can be computed via Eq. (17).

3.3. Results

Here, we consider a reservoir-pipe-valve system with pipe length $l = 1000$ m and internal diameter $d = 0.5$ m. The wave speed is $a = 1200$ m/s and the Darcy–Weisbach friction factor is $f_{DW} = 0.02$. The pressure head at the upstream reservoir x^U is $H(x^U) = 25$ m. Here, $J = 151$ frequencies from ω_{th} to $15\omega_{th}$ are selected, where $\omega_{th} = a\pi/(2l) = 1.89$ rad/s is the fundamental angular frequency. Therefore, the minimum wavelength is $\lambda_{\min} = 2\pi a/(15\omega_{th}) = 267$ m.

The optimal location of the first sensor is decided by the objective function in Eq. (19). Here, the leak location is assumed to follow a uniform distribution $\mathrm{U}(\mathcal{X})$ with PDF $f_x(x^L) = 1/l, x^L \in [0, l]$. The leak size is also uniformly distributed with maximum $s^L_{\max} = 5 \times 10^{-4}$ m^2. The sample size K of Sobol' sequence is 500 which guarantees the convergence. The objective function in Eq. (19) versus the sensor location is plotted by the black curve in Fig. 2, in which the vertical dash lines are plotted with equal distance $\lambda_{\min}/4$. This figure shows that the optimal measurement location is the downstream end of the pipe x^D, i.e., at the wave generator. Furthermore, the sensor cannot be placed near $x^U = 0$ which leads to an infinite leak localization error. This is because x^U is connected to a reservoir where the pressure is constant and the oscillation of transient wave cannot be sensed.

Then, subsequent sensors are added in the system. First, the sensor ambiguity issue is illustrated. The leak is assumed to be located at $x^L = 200$ m and the locations of two sensors are free parameters. The normalized ambiguity function [40] of the pressure head from the two sensors:

$$AMS(x_1^S, x_2^S) = \frac{|\mathbf{h}^H(x_1^S)\mathbf{h}(x_2^S)|}{\|\mathbf{h}(x_1^S)\|\|\mathbf{h}(x_2^S)\|} \tag{37}$$

is plotted in Fig. 3, which clearly shows a diagonal band with very high similarity. The width of the diagonal band is approximately $\lambda_{\min}/2$, which implies that if the distance between the two sensors is lower than $\lambda_{\min}/2$, the measurements have a strong similarity. This is undesired for the leak estimation and, thus, also undesired for the design of multiple sensors, as has been indicated in Section 2.3. Furthermore, we justify that, when $M = 2$, deciding the second sensor x_2^S via Eq. (20) (without changing the first sensor x_1^S obtained from Eq. (19)) is optimal and equivalent to optimizing x_2^S and x_1^S simultaneously. Fig. 4 plots the CRLB versus x_1^S and x_2^S, which demonstrates that the optimal points are all located at the upper and right boundaries, i.e., $x_1^S = \widehat{x_1^S} = l$.

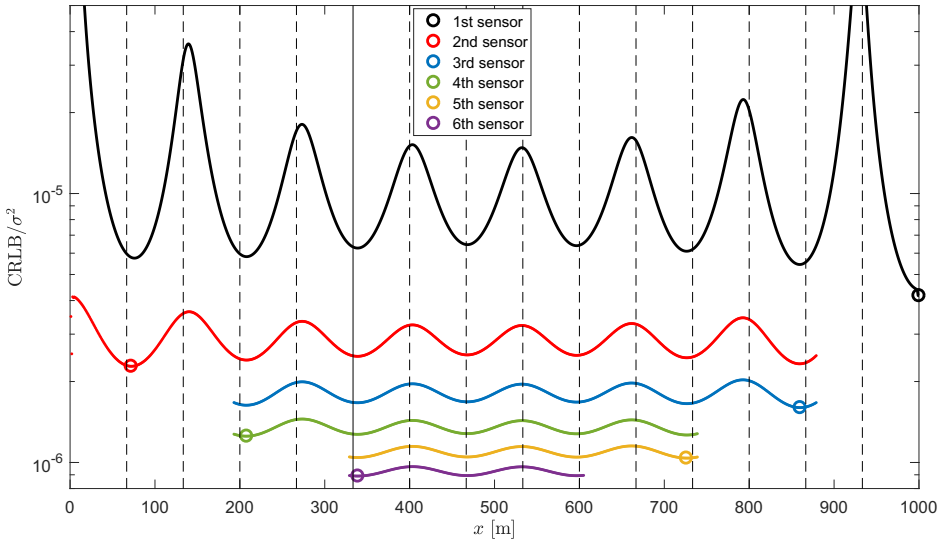

Fig. 2. CRLB normalized by σ^2 versus sensor locations. The maximum angular frequency is $\omega_{\max} = 15\omega_{th}$. The dash lines represent $x = nl\omega_{th}/\omega_{\max} = n\lambda_{\min}/4 = nl/15, n = 1, 2, \ldots, 14$.

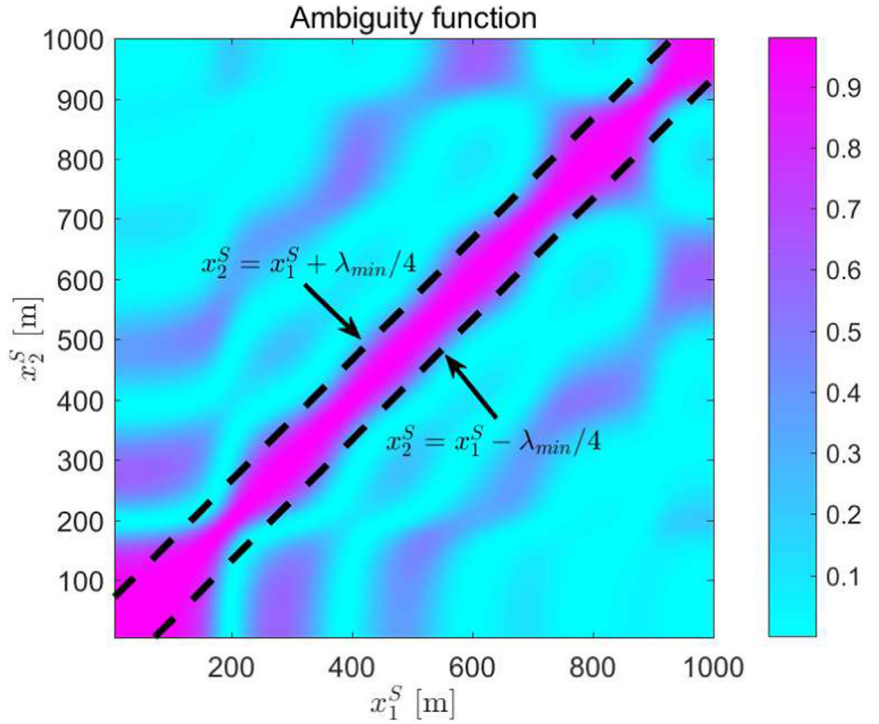

Fig. 3. The normalized ambiguity function versus the locations of two sensors. The region between the two dash lines represents the distance between the two sensors lower than $\lambda_{min}/2$.

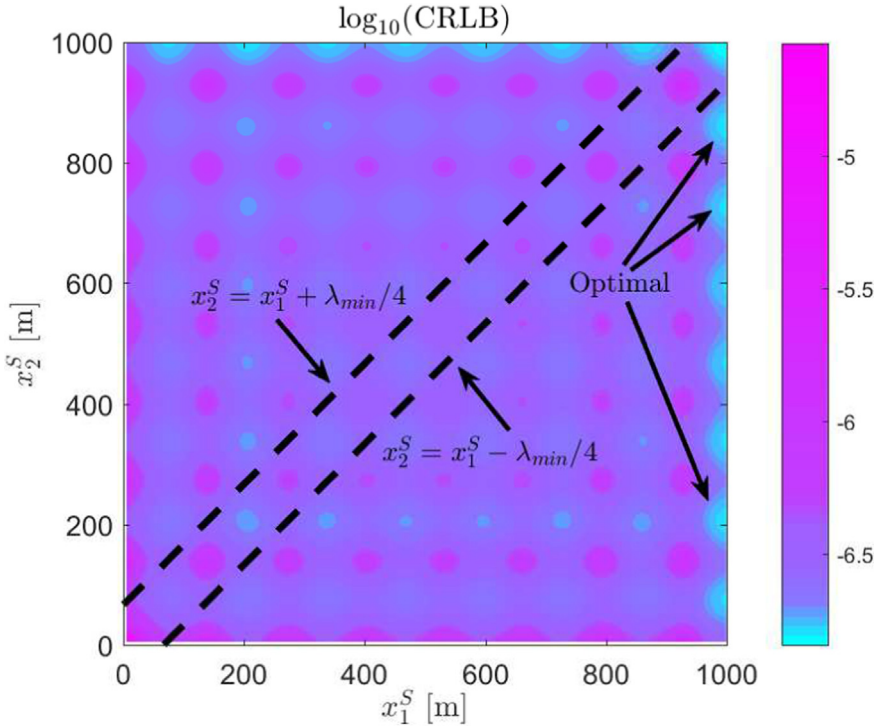

Fig. 4. CRLB versus the locations of two sensor. The region between the two dash lines represents the distance between the two sensors lower than $\lambda_{min}/2$.

The optimal locations of the second to sixth sensors are computed via Eq. (20) and displayed in Fig. 2. It is suggested that the sensors are placed with distance approximately $\lambda_{\min}/2$ and, sequentially, from downstream side and then upstream side. Note that, in practice, the maximum frequency or minimum wavelength of transient wave is controllable and decided by the time closure of valve t_c ($\lambda_{\min} \approx at_c$). Moreover, the raw data are often post-processed before the leakage localization, which automatically decides the frequency range of data more precisely, using the low-pass filter for noise reduction [61] or the frequency selection which is a must for using the frequency domain leakage localization methods [8,9].

4. Pipe networks

4.1. Physical model

A general pipe network $\mathcal{X}$ composed of P pipes and N nodes is considered. As shown in Fig. 5, the nodes in a network are divided into two classes: (i) ends or boundaries of the network, denoted by $\partial\mathcal{X}$, which are those nodes connected to only one pipe, including one boundary where the wave-generation valve is set (denoted by $\mathcal{V}$); (ii) interior junctions, denoted by $\mathcal{I}$, which are the nodes connected to at least two pipes. For simplicity, a node connecting to exactly two pipes is considered as an interior junction only if the two pipes have different properties (e.g., diameter, thickness, or material), which results in a change of impedance and wave reflections at this node; otherwise, it is just an ordinary interior point. Let the numbers of ends and interior junctions be $N_E = \mathrm{card}(\partial\mathcal{X})$ and $N_I = \mathrm{card}(\mathcal{I})$, where "card" represents the cardinality of a set, thus $N_E + N_I = N$. Let x_p denote the coordinate in the p-th pipe, which is bounded by x_p^U and $x_p^D, p = 1, \ldots, P$. Thus, the whole network is denoted by $\mathcal{X} = \cup_{p=1}^{P}\left\{x_p : x_p \in \left[x_p^U, x_p^D\right]\right\}$. Furthermore, the length, diameter and cross-sectional area of the p-th pipe are l_p, d_p and A_p, respectively.

The wave propagation from the upstream x_p^U to the downstream x_p^D in the p-th pipe is modeled by the transfer matrix

$$\begin{pmatrix} q\left(x_p^D\right) \\ h\left(x_p^D\right) \end{pmatrix} = \mathbf{M}^{x_p^U \to x_p^D} \begin{pmatrix} q\left(x_p^U\right) \\ h\left(x_p^U\right) \end{pmatrix}, \ p = 1, \ldots, P. \tag{38}$$

When the leak is in the p^*-th pipe, $p^* \in \{1, \ldots, P\}$,

$$\mathbf{M}^{x_{p^*}^U \to x_{p^*}^D} = \mathbf{M}^{NSL}\left(x^L, s^L, x_{p^*}^U, x_{p^*}^D\right), \tag{39}$$

and

$$\mathbf{M}^{x_p^U \to x_p^D} = \mathbf{M}^{NL}\left(x_p^D - x_p^U\right), p \neq p^* \text{ and } p \in \{1, \ldots, P\}. \tag{40}$$

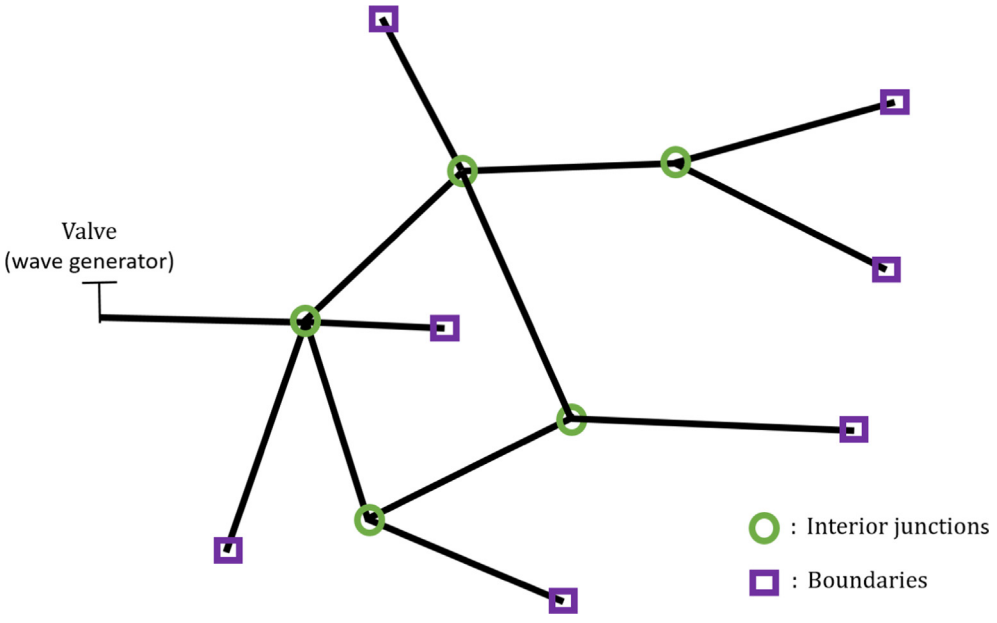

Fig. 5. Sketch map of a pipe network.

Here, we denote

$$\mathbf{M}^{NSL}(x^L, s^L, x^U, x^D) = \mathbf{M}^{NL}(x^D - x^U) + s^L \mathbf{M}^{SL}(x^L, x^U, x^D). \tag{41}$$

For each end $x^E \in \partial\mathcal{X}$, a boundary condition is assumed. If $x^E = \mathcal{V}$ is the valve which generates transient waves,

$$q(x^E) = 1. \tag{42}$$

For each $x^E \in \partial\mathcal{X}/\mathcal{V}$, the following three types of boundary condition are considered:

- if x^E is connected to a reservoir,

$$h(x^E) = 0; \tag{43}$$

- if x^E is a dead-end,

$$q(x^E) = 0; \tag{44}$$

- if x^E is a complex dynamic boundary (e.g., a pressure reducing valve is set), a pressure sensor can be installed at x^E such that $h(x^E)$ can be measured [55].

For each interior junction $x^J \in \mathcal{I}$, it is connected to N_J ($N_J \geqslant 2$) pipes and the adjoint (limiting) point in the n_J-th pipe ($n_J = 1, \ldots, N_J$) is denoted by $x^J_{n_J}$. By the equilibrium of pressure and conservation of mass across the junction, we have

$$h\left(x^J_1\right) = h\left(x^J_2\right) = \cdots = h\left(x^J_{N_J}\right) \tag{45}$$

and

$$\sum_{n_J=1}^{N_J} (-1)^{\alpha_{n_J}} q\left(x^J_{n_J}\right) = 0, \tag{46}$$

where $\alpha_{n_J} = 0$ if it is inflow (the flow direction is from the n_J-th pipe toward x^J) and $\alpha_{n_J} = 1$ in the case of outflow.

In a network with P pipes, $q\left(x^U_p\right), h\left(x^U_p\right), q\left(x^D_p\right)$ and $h\left(x^D_p\right), p = 1, \ldots, P$, can be uniquely solved by a system of $4P$ linear equations with a matrix form:

$$\mathbf{My} = \mathbf{b}, \tag{47}$$

where

$$\mathbf{b} = (0, \ldots, 0, 1)^\top \tag{48}$$

and

$$\mathbf{y} = \left(q(x^U_1), h(x^U_1), q(x^D_1), h(x^D_1), \ldots, q(x^U_P), h(x^U_P), q(x^D_P), h(x^D_P)\right)^\top. \tag{49}$$

The first $2P$ equations are from the transfer matrix Eq. (38); the first $2P$ lines of $\mathbf{M}$ are

$$\begin{pmatrix} \mathbf{M}^{x^U_1 \to x^D_1} & -\mathbf{I} & \cdots & \cdots & \mathbf{0} & \mathbf{0} \\ \cdots & \cdots & \cdots & \cdots & \cdots & \cdots \\ \mathbf{0} & \mathbf{0} & \cdots & \cdots & \mathbf{M}^{x^U_P \to x^D_P} & -\mathbf{I} \end{pmatrix}. \tag{50}$$

The other $2P$ equations are obtained from the N_I boundary conditions for the interior nodes in $\mathcal{I}$ from Eqs. (45) and (46), the $2P - N_I - 1$ boundary conditions for the ends in $\partial\mathcal{X}/\mathcal{V}$ from Eq. (43) or (44), and one boundary condition (the last line of $\mathbf{M}$) obtained from Eq. (42).

Solving $\mathbf{y} = \mathbf{M}^{-1}\mathbf{b}$, the discharge q and pressure head h at each end of each pipe are obtained, then q and h at any location in the network can be computed. For a sensor located at $x^S_m \in \left(x^U_p, x^D_p\right)$ in the p-th pipe,

$$\begin{pmatrix} q\left(x^S_m\right) \\ h\left(x^S_m\right) \end{pmatrix} = \mathbf{M}^{x^U_p \to x^S_m} \begin{pmatrix} q\left(x^U_p\right) \\ h\left(x^U_p\right) \end{pmatrix}, \tag{51}$$

where

$$\mathbf{M}^{x^U_p \to x^S_m} = \mathbf{M}^{NSL}\left(x^L, s^L, x^U_p, x^S_m\right) \tag{52}$$

if x^L is located in the p-th pipe and between x^U_p and x^S_m; otherwise

$$\mathbf{M}^{x_p^U \to x_m^S} = \mathbf{M}^{NL}\left(x_m^S - x_p^U\right). \tag{53}$$

4.2. CRLB computation

In theory, the pressure head at any location can be analytically solved via Eq. (51), then the partial derivatives $\frac{\partial h_{mj}^{model}}{\partial x^L}$ and $\frac{\partial h_{mj}^{model}}{\partial s^L}$, as well as the CRLB, can also be analytically derived, as the case of single pipe in Section 3.2. However, this is complicated especially for complex networks. For example, $q\left(x_p^U\right), h\left(x_p^U\right), q\left(x_p^D\right)$ and $h\left(x_p^D\right), p = 1, \ldots, P$, have to be solved by inverting the system of linear equations (with $4P$ equations and $4P$ unknowns) analytically. Alternatively, in this section, a numerical approach for computing the partial derivatives is employed. The detailed procedure of CRLB computation is given in Algorithm 2.

Algorithm 2 CRLB computation (specification of Line 5 and Line 12 in Algorithm 1) in a pipe network.

1: For each QMC sample $x_{(k)}^L$ and $s_{(k)}^L$, if $x_{(k)}^L$ is in p^*-th pipe ($p^* \in \{1, \ldots, P\}$), derive the analytical form of $\mathbf{M}^{x_{p^*}^U \to x_{p^*}^D}$ from Eq. (39) and $\mathbf{M}^{x_p^U \to x_p^D}$ (for $p = 1, \ldots, p^* - 1, p^* + 1, \ldots, P$) from Eq. (40), then insert them into $\mathbf{M}$ by Eq. (50);

2: Derive $q\left(x_p^U\right), h\left(x_p^U\right), q\left(x_p^D\right)$ and $h\left(x_p^D\right), p = 1, \ldots, P$, by solving the inverse of Eq. (47), i.e., $\mathbf{y} = \mathbf{M}^{-1}\mathbf{b}$;

3: Obtain $h_{mj}^{model}\left(x_{(k)}^L, s_{(k)}^L\right)$ from the second line of Eq. (51) for each $x_m^S \in \mathcal{X}$;

4: Repeat 1–3 to obtain $h_{mj}^{model}\left(x_{(k)}^L + \epsilon_x, s_{(k)}^L\right)$ with a small ϵ_x;

5: Repeat 1–3 and obtain $h_{mj}^{model}\left(x_{(k)}^L, s_{(k)}^L + \epsilon_s\right)$ with a small ϵ_s;

6: Compute the derivatives by

$$\frac{\partial h_{mj}^{model}}{\partial x^L}\left(x_{(k)}^L, s_{(k)}^L\right) = \frac{h_{mj}^{model}\left(x_{(k)}^L + \epsilon_x, s_{(k)}^L\right) - h_{mj}^{model}\left(x_{(k)}^L, s_{(k)}^L\right)}{\epsilon_x} \tag{54}$$

and

$$\frac{\partial h_{mj}^{model}}{\partial s^L}\left(x_{(k)}^L, s_{(k)}^L\right) = \frac{h_{mj}^{model}\left(x_{(k)}^L, s_{(k)}^L + \epsilon_s\right) - h_{mj}^{model}\left(x_{(k)}^L, s_{(k)}^L\right)}{\epsilon_s}; \tag{55}$$

7: Compute the CRLB via Eq. (17).

4.3. Examples and results

In this section, simple branched and looped pipe systems, which form the basic topological structures of any complex pipe network, are first studied. In addition, a classical example of pipe network is revisited, by which the interests of the proposed sensor design approach are demonstrated.

4.3.1. Branched system with three pipes

A branched pipe system composed of three pipes is considered and shown in Fig. 6. Here, x_1^D, x_2^D, and x_3^U are all located at the interior junction of the system, but they stand for locations in different pipes approaching the junction: x_1^D and x_2^D are just upstream of the junction in Pipe 1 and Pipe 2, respectively; x_3^U is just downstream of the junction in Pipe 3. The wave propagation in the three pipes is described by the field transfer matrix by Eq. (38). It is assumed that x_1^U and x_2^U are connected to reservoirs and x_3^D is a valve (wave generator), thus the following boundary condition are enforced:

$$h(x_1^U) = 0; h(x_2^U) = 0; q(x_3^D) = 1. \tag{56}$$

The steady-state flow direction in each pipe is shown in Fig. 6, by which the relationship of discharge and pressure head at the interior junction is

$$q(x_1^D) + q(x_2^D) - q(x_3^U) = 0; h(x_1^D) = h(x_2^D) = h(x_3^U). \tag{57}$$

Writing the 12 linear equations in the matrix form, a specific form of Eq. (47) is derived:

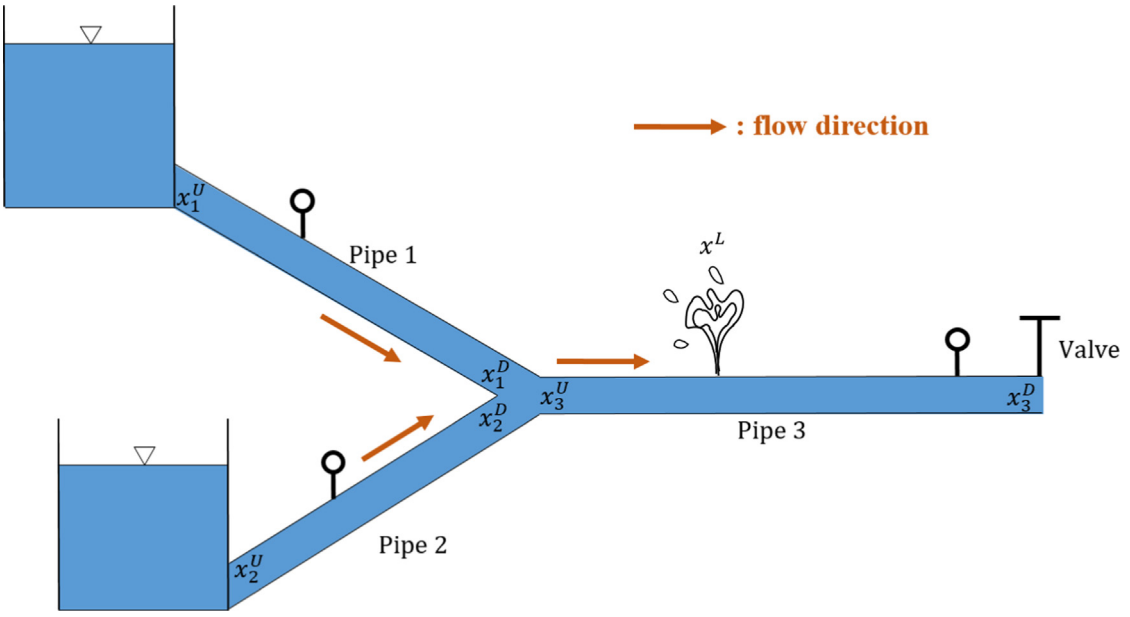

Fig. 6. A branched pipe system composed of three pipes.

$$\begin{pmatrix} \mathbf{M}^{x_1^U \to x_1^D} & -\mathbf{I} & \mathbf{0} & \mathbf{0} & \mathbf{0} & \mathbf{0} \\ \mathbf{0} & \mathbf{0} & \mathbf{M}^{x_2^U \to x_2^D} & -\mathbf{I} & \mathbf{0} & \mathbf{0} \\ \mathbf{0} & \mathbf{0} & \mathbf{0} & \mathbf{0} & \mathbf{M}^{x_3^U \to x_3^D} & -\mathbf{I} \\ 0\ 0 & 0\ 1\ 0\ 0 & 0\ 0 & 0 & -1 & 0\ 0 \\ 0\ 0 & 0\ 0\ 0\ 0 & 0\ 1 & 0 & -1 & 0\ 0 \\ 0\ 0 & 1\ 0\ 0\ 0 & 1\ 0 & -1 & 0 & 0\ 0 \\ 0\ 1 & 0\ 0\ 0\ 0 & 0\ 0 & 0 & 0 & 0\ 0 \\ 0\ 0 & 0\ 0\ 0\ 1 & 0\ 0 & 0 & 0 & 0\ 0 \\ 0\ 0 & 0\ 0\ 0\ 0 & 0\ 0 & 0 & 0 & 1\ 0 \end{pmatrix} \begin{pmatrix} q(x_1^U) \\ h(x_1^U) \\ q(x_1^D) \\ h(x_1^D) \\ q(x_2^U) \\ h(x_2^U) \\ q(x_2^D) \\ h(x_2^D) \\ q(x_3^U) \\ h(x_3^U) \\ q(x_3^D) \\ h(x_3^D) \end{pmatrix} = \begin{pmatrix} 0 \\ 0 \\ 0 \\ 0 \\ 0 \\ 0 \\ 0 \\ 0 \\ 0 \\ 0 \\ 0 \\ 1 \end{pmatrix}. \tag{58}$$

By solving $\mathbf{M}^{-1}\mathbf{b}$, $q\left(x_p^U\right), h\left(x_p^U\right), q\left(x_p^D\right)$ and $h\left(x_p^D\right), p = 1, 2, 3$, are obtained, then the pressure head at any location in the p-th pipe is given by Eq. (51).

Then, the system parameters are explicitly given and the results of sensor placement design are presented. The lengths of the three pipes are $l_1 = 600$ m, $l_2 = 400$ m and $l_3 = 500$ m. The internal diameter of pipe is $d_1 = d_2 = d_3 = 0.5$ m. The wave speed is $a = 1200$ m/s and the Darcy–Weisbach friction factor is $f_{DW} = 0.02$. The steady-state pressure head at the upstream reservoir x_1^U is $H(x_1^U) = 25$ m. The maximum frequency is assumed to be $15\omega_{th}$ where $\omega_{th} = a\pi/(2(l_1 + l_3))$. The leak location x^L is assumed to follow the uniform distribution with PDF

$$f_x(x^L) = \frac{1}{l_1 + l_2 + l_3}, x^L \in \mathcal{X}. \tag{59}$$

The leak size is also uniformly distributed as in Section 3.3. The optimal locations of the first four sensors are displayed in Fig. 7. The first sensor is, again, located at the valve, while the second to the fourth sensors are suggested to be placed in the three pipes, respectively.

4.3.2. Looped system with four pipes

A looped pipe system with four pipes is considered; the setup is shown in Fig. 8. At the two junctions, the discharge and head have the relationship:

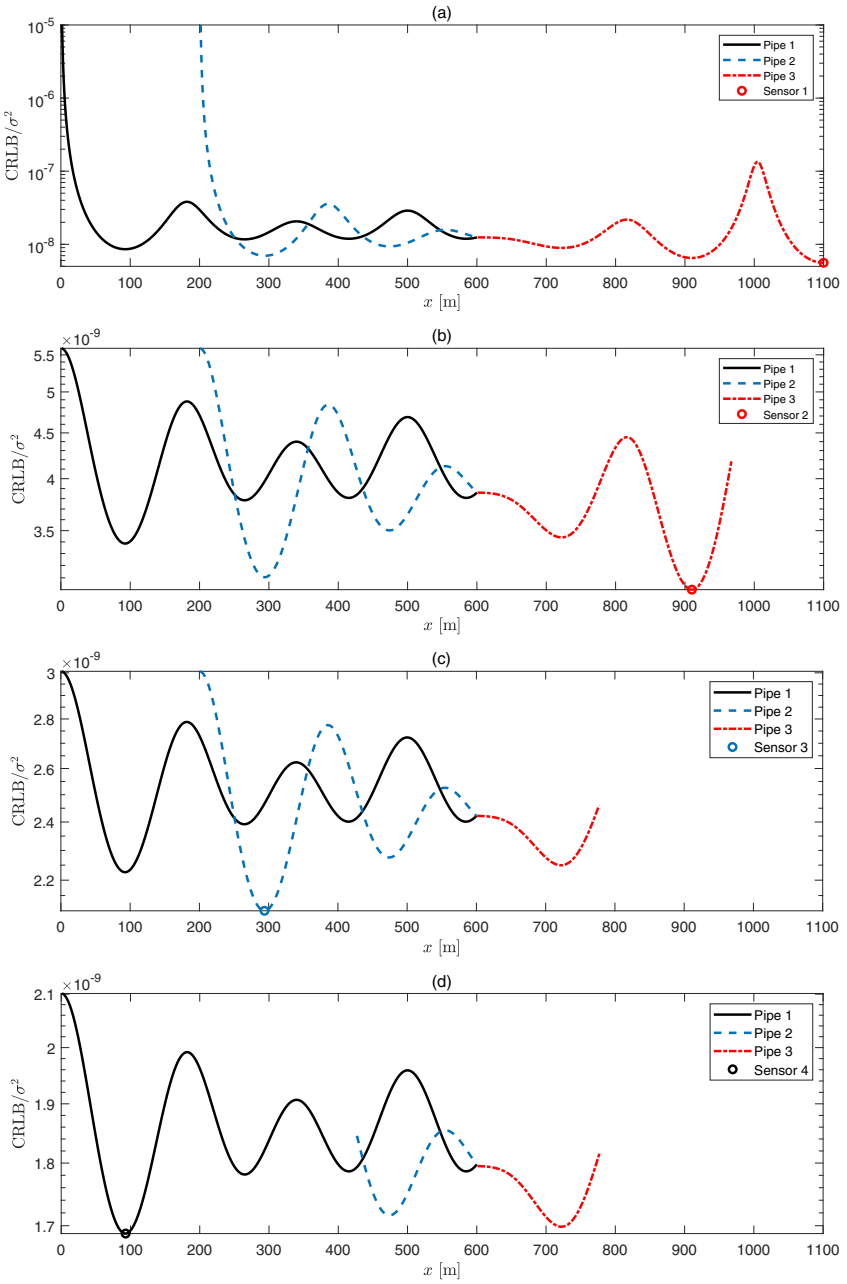

Fig. 7. CRLB normalized by σ^2 for the branched pipe system.

$$q(x_1^D) - q(x_2^U) - q(x_3^U) = 0, h(x_1^D) = h(x_2^U) = h(x_3^U); \tag{60}$$

$$q(x_2^D) + q(x_3^D) - q(x_4^U) = 0, h(x_2^D) = h(x_3^D) = h(x_4^U). \tag{61}$$

Since x_1^U is connected to a reservoir and x_4^D is a valve which generates transient wave by sudden valve closing/opening, thus the following boundary condition are enforced:

$$h(x_1^U) = 0; q(x_4^D) = 1. \tag{62}$$

The system of 16 linear equations in the matrix form is

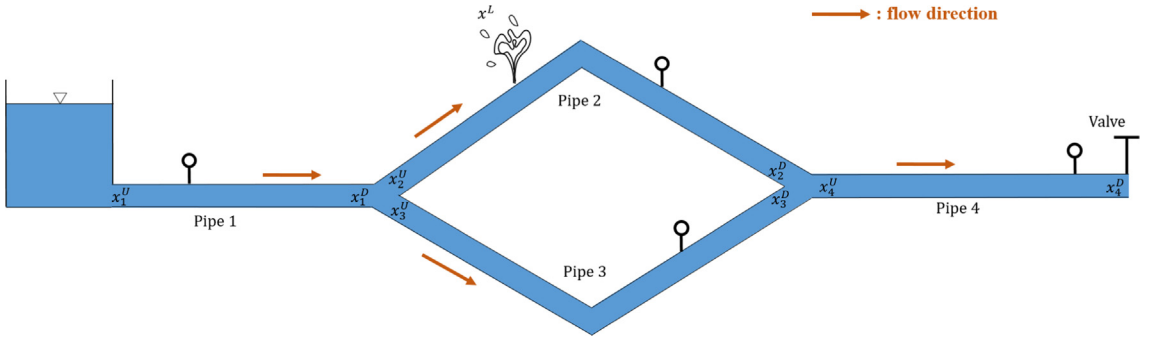

Fig. 8. A looped pipe system with four pipes.

$$\begin{pmatrix} \mathbf{M}^{x_1^U\to x_1^D} & -\mathbf{I} & \mathbf{0} & \mathbf{0} & \mathbf{0} & \mathbf{0} & \mathbf{0} & \mathbf{0} \\ \mathbf{0} & \mathbf{0} & \mathbf{M}^{x_2^U\to x_2^D} & -\mathbf{I} & \mathbf{0} & \mathbf{0} & \mathbf{0} & \mathbf{0} \\ \mathbf{0} & \mathbf{0} & \mathbf{0} & \mathbf{0} & \mathbf{M}^{x_3^U\to x_3^D} & -\mathbf{I} & \mathbf{0} & \mathbf{0} \\ \mathbf{0} & \mathbf{0} & \mathbf{0} & \mathbf{0} & \mathbf{0} & \mathbf{0} & \mathbf{M}^{x_4^U\to x_4^D} & -\mathbf{I} \\ 0\ 0 & 0\ 1 & 0\ -1 & 0\ 0 & 0\ 0 & 0\ 0 & 0\ 0 & 0\ 0 \\ 0\ 0 & 0\ 1 & 0\ 0 & 0\ 0 & 0\ -1 & 0\ 0 & 0\ 0 & 0\ 0 \\ 0\ 0 & 1\ 0 & -1\ 0 & 0\ 0 & -1\ 0 & 0\ 0 & 0\ 0 & 0\ 0 \\ 0\ 0 & 0\ 0 & 0\ 0 & 0\ 1 & 0\ 0 & 0\ -1 & 0\ 0 & 0\ 0 \\ 0\ 0 & 0\ 0 & 0\ 0 & 0\ 0 & 0\ 1 & 0\ -1 & 0\ 0 & 0\ 0 \\ 0\ 0 & 0\ 0 & 0\ 0 & 0\ 1 & 0\ 0 & 1\ 0 & -1\ 0 & 0\ 0 \\ 0\ 1 & 0\ 0 & 0\ 0 & 0\ 0 & 0\ 0 & 0\ 0 & 0\ 0 & 0\ 0 \\ 0\ 0 & 0\ 0 & 0\ 0 & 0\ 0 & 0\ 0 & 0\ 0 & 0\ 1 & 0\ 0 \end{pmatrix} \begin{pmatrix} q(x_1^U) \\ h(x_1^U) \\ q(x_1^D) \\ h(x_1^D) \\ q(x_2^U) \\ h(x_2^U) \\ q(x_2^D) \\ h(x_2^D) \\ q(x_3^U) \\ h(x_3^U) \\ q(x_3^D) \\ h(x_3^D) \\ q(x_4^U) \\ h(x_4^U) \\ q(x_4^D) \\ h(x_4^D) \end{pmatrix} = \begin{pmatrix} 0 \\ 0 \\ 0 \\ 0 \\ 0 \\ 0 \\ 0 \\ 0 \\ 0 \\ 0 \\ 0 \\ 0 \\ 0 \\ 0 \\ 0 \\ 1 \end{pmatrix} \tag{63}$$

The lengths of the four pipes are $l_1 = 450$ m, $l_2 = 350$ m, $l_3 = 350$ m and $l_4 = 400$ m. The pipe diameters are $d_1 = 0.5$ m, $d_2 = 0.35$ m, $d_3 = 0.15$ m and $d_4 = 0.5$ m. The pressure head at the upstream reservoir is $H(x_1^U) = 25$ m. The wave speed is $a = 1200$ m/s and the Darcy–Weisbach friction factor is $f_{DW} = 0.02$. The maximum frequency is assumed to be $15\omega_{th}$ where $\omega_{th} = a\pi/(2(l_1 + l_2 + l_4))$. The PDF of leak location is assumed to be

$$f_x(x^L) = \begin{cases} \frac{1}{l_1+l_2+l_4}, x^L \in \left[x_1^U, x_1^D\right] \cup \left[x_2^U, x_2^D\right] \cup \left[x_4^U, x_4^D\right] \\ 0, x^L \in \left[x_3^U, x_3^D\right] \end{cases}, \tag{64}$$

i.e., we believe that Pipe 3 has no leak and the other three pipes have equal chance to have a leak. This can be a case that Pipe 3 is newly-built but the other pipes are aging. The optimal locations of the first five sensors are displayed in Fig. 9. In this case, the first choice is not the location of the valve but in Pipe 2. The first five sensors are assigned to each of the four pipes. Although it is assumed that no leak can appear in Pipe 3, it is still suggested to install a sensor in this pipe, where the measured signal includes sufficient information of leak propagated from other pipes.

4.3.3. A complex network

In this section, a pipe network with 11 pipes and 7 nodes, which has been previously investigated for sensor location design in [31,32,34], is revisited. Note that in [31,32,34] the sensors and leaks can only be located at the 7 nodes, which is not realistic for real pipe networks. In the following, the design is for sensors that can be placed at anywhere in the 11 pipes and considers all the possible leak locations throughout the network.

The setup of the network is shown in Fig. 10. The coordinate system is $\mathcal{X} = \cup_{p=1}^{11}\left\{x_p : x_p \in \left[x_p^U, x_p^D\right]\right\}$ where $x_p^U = 0$ is the upstream and $x_p^D = l_p$ is the downstream boundary of the p-th pipe. The boundary conditions at the 7 nodes (in total 22 equalities) are:

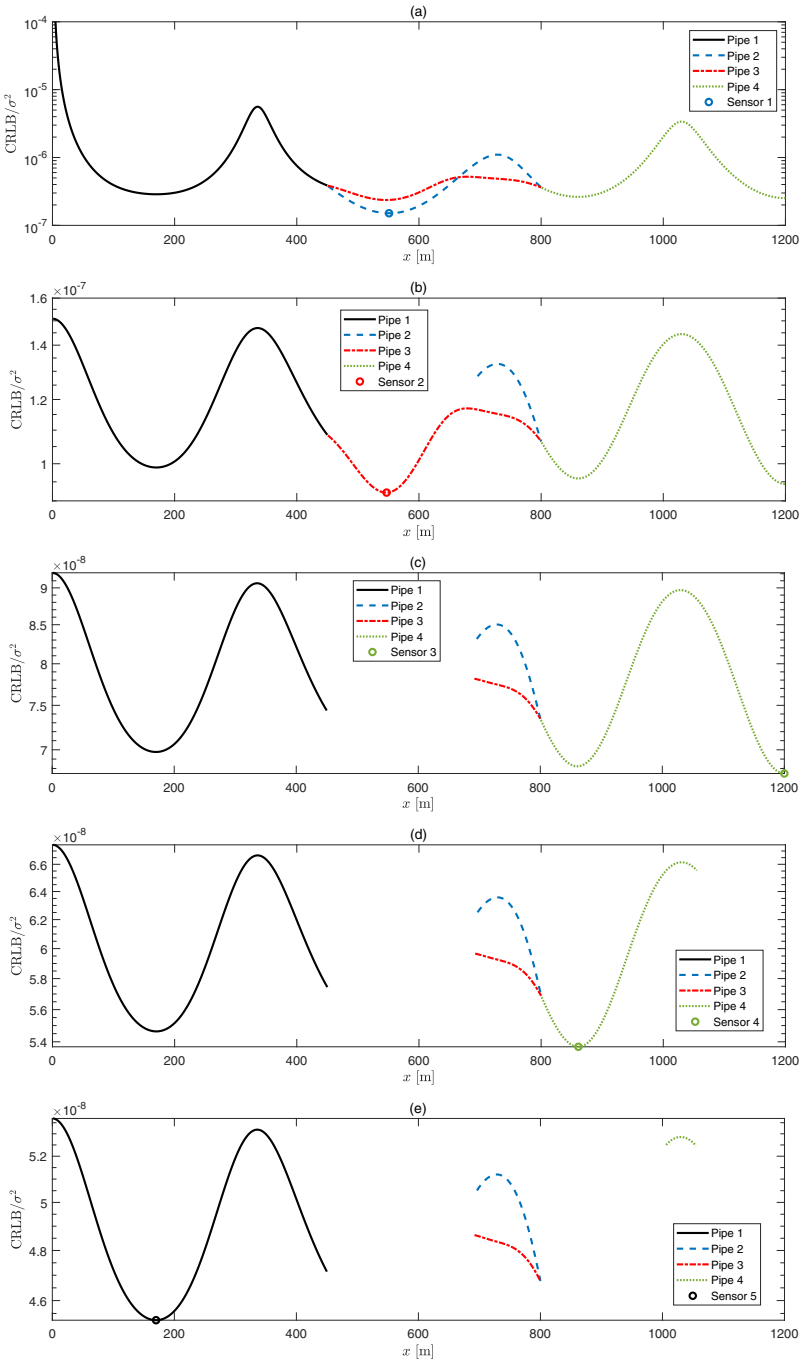

Fig. 9. CRLB normalized by σ^2 for the looped pipe system.

$$h(x_1^U) = 0, h(x_2^U) = 0; \tag{65}$$

$$h(x_1^D) = h(x_3^U) = h(x_4^U) = h(x_5^U), q(x_1^D) = q(x_3^U) + q(x_4^U) + q(x_5^U); \tag{66}$$

$$h(x_2^D) = h(x_3^D) = h(x_{10}^U) = h(x_{11}^U), q(x_2^D) + q(x_3^D) = q(x_{10}^U) + q(x_{11}^U); \tag{67}$$

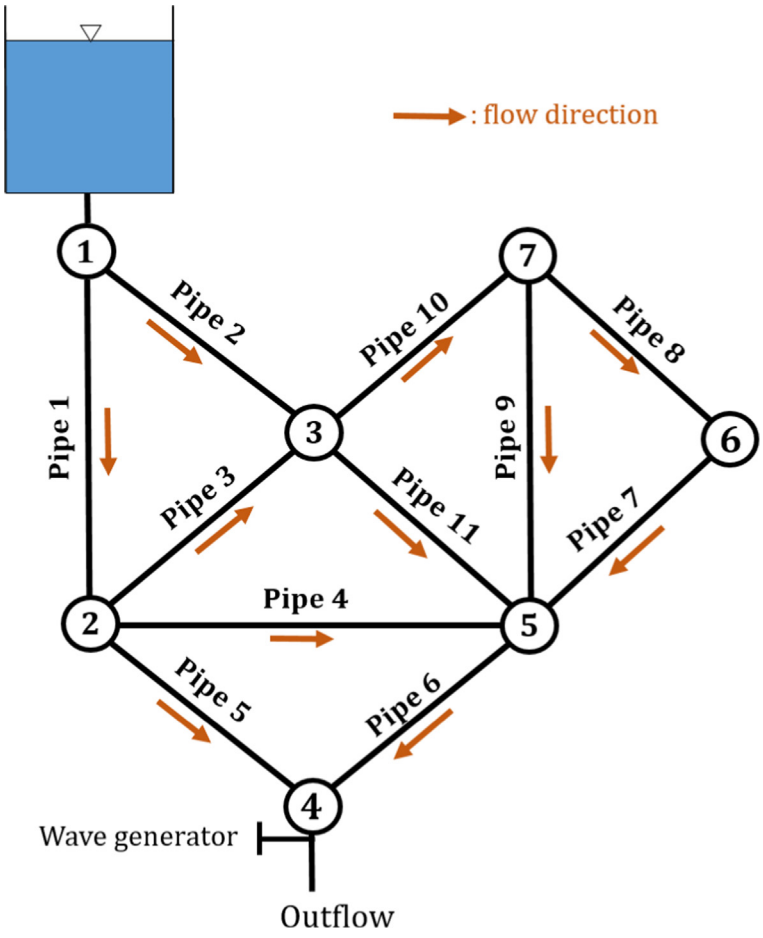

Fig. 10. A pipe network with 11 pipes and 7 nodes.

$$h(x_5^D) = h(x_6^D), q(x_5^D) + q(x_6^D) = 1; \tag{68}$$

$$h(x_{11}^D) = h(x_9^D) = h(x_7^D) = h(x_4^D) = h(x_6^U), q(x_{11}^D) + q(x_9^D) + q(x_7^D) + q(x_4^D) = q(x_6^U); \tag{69}$$

$$h(x_8^D) = h(x_7^U), q(x_8^D) = q(x_7^U); \tag{70}$$

$$h(x_{10}^D) = h(x_9^U) = h(x_8^U), q(x_{10}^D) = q(x_9^U) + q(x_8^U). \tag{71}$$

Along with the 22 equalities in the transfer matrix Eq. (38) for $p = 1, \ldots, 11$, the system is uniquely solved.

The system parameters in [31] are used. All of the 11 pipes share a common diameter of $d_p = 0.254$ m, a common length of $l_p = 762$ m, and a common wave speed of $a = 1316$ m/s. The steady-state flow is 20 L/s. The leak location is assumed to follow the uniform distribution, i.e., the PDF of x^L is

$$f_x(x^L) = 1/\sum_{p=1}^{P} l_p, x^L \in \mathcal{X}. \tag{72}$$

The maximum frequency is $10\omega_{th}$, where $\omega_{th} = a\pi/(2l_p)$. The CRLB versus the first sensor location throughout the network $\mathcal{X}$ is shown in Fig. 11. The optimal location of the first sensor is $x_9 = 383$ m in Pipe 9 and the optimal locations of the first 20 sensors are given in Table 1. It is clear that in general the nodes are not the optimal measurement locations and the proposed method is able to design a sensor system with more accurate leak detection than the methods in [31,32,34].

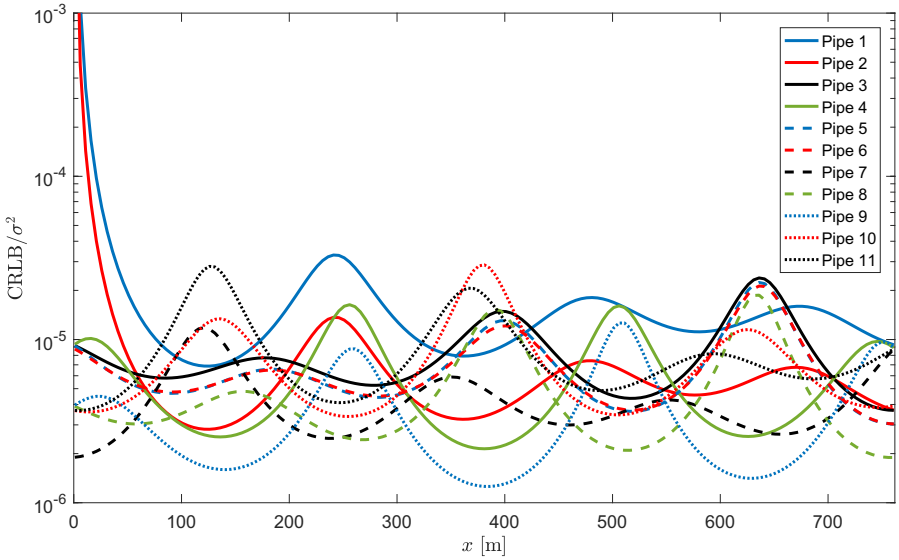

Fig. 11. Normalized CRLB versus first sensor location in the 11 pipes of the network.

Table 1
Optimal locations of the first 20 sensors in the pipe network.

Sensor No.	Location	Sensor No.	Location
1	383 m in Pipe 9	11	656 m in Pipe 7
2	630 m in Pipe 9	12	123 m in Pipe 2
3	142 m in Pipe 9	13	459 m in Pipe 7
4	Node 6	14	57 m in Pipe 8
5	515 m in Pipe 8	15	Node 4
6	381 m in Pipe 4	16	363 m in Pipe 2
7	267 m in Pipe 8	17	256 m in Pipe 10
8	239 m in Pipe 7	18	505 m in Pipe 10
9	136 m in Pipe 4	19	Node 3
10	626 m in Pipe 4	20	Node 7

5. Conclusion

This paper studies the optimal strategy of sensor placement in water supply pipe networks for the purpose of leak detection. The proposed methodology determines the optimal measurement locations by maximizing the measurement information about leaks with respect to pipe network coordinate. Explicit algorithm for computing the Fisher information and Cramér–Rao lower bound (CRLB) in a general pipe network is developed. A probabilistic framework to model the randomness of the appearance of leaks is proposed. The stochastic simulation of transient wave propagation, the consequent CRLB and the optimal distribution of sensors with consideration of the random leaks are realized via the quasi-Monte-Carlo simulations. Examples from the simple single-pipe system to the complex pipe network are presented to illustrate the efficiency of the proposed methodology.

In the present paper, the mismatch between the transient data and model is assumed to be a Gaussian-distributed random error. In real-life pipe networks where more complex uncertainties may exist, the influence of each random model parameter can also be modeled, such that the uncertainties in the data are more precisely quantified. This needs a careful study of the stochastic characteristics of the parameters in the transient model and a generalization of the sensor design methodology, which should be able to quantify both the measurement error and the system parameter uncertainties.

CRediT authorship contribution statement

Xun Wang: Conceptualization, Methodology, Software, Data curation, Visualization, Writing - original draft, Writing - review & editing.

Declaration of Competing Interest

The author declares that he has no known competing financial interests or personal relationships that could have appeared to influence the work reported in this paper.

Acknowledgement

This work has been supported by research grants from the Special Project of Double First Class University Plan (No.: ZG216S2080) and the Guangxi Natural Science Foundation (No.: 2018GXNSFBA281013).

References

[1] R. Liemberger, A. Wyatt, Quantifying the global non-revenue water problem, Water Supply 19 (3) (2019) 831–837.
[2] A.F. Colombo, P. Lee, B.W. Karney, A selective literature review of transient-based leak detection methods, Journal of Hydro-Environment Research 2 (4) (2009) 212–227.
[3] J.A. Liggett, L.-C. Chen, Inverse transient analysis in pipe networks, Journal of Hydraulic Engineering 120 (8) (1994) 934–955.
[4] B. Brunone, Transient test-based technique for leak detection in outfall pipes, Journal of Water Resources Planning and Management 125 (5) (1999) 302–306.
[5] J.P. Vítkovskỳ, A.R. Simpson, M.F. Lambert, Leak detection and calibration using transients and genetic algorithms, Journal of Water Resources Planning and Management 126 (4) (2000) 262–265.
[6] S.T.N. Nguyen, J. Gong, M.F. Lambert, A.C. Zecchin, A.R. Simpson, Least squares deconvolution for leak detection with a pseudo random binary sequence excitation, Mechanical Systems and Signal Processing 99 (2018) 846–858.
[7] M. Ferrante, B. Brunone, S. Meniconi, Wavelets for the analysis of transient pressure signals for leak detection, Journal of Hydraulic Engineering 133 (11) (2007) 1274–1282.
[8] P.J. Lee, J.P. Vítkovskỳ, M.F. Lambert, A.R. Simpson, J.A. Liggett, Leak location using the pattern of the frequency response diagram in pipelines: a numerical study, Journal of Sound and Vibration 284 (3) (2005) 1051–1073.
[9] X. Wang, M.S. Ghidaoui, Pipeline leak detection using the matched-field processing method, Journal of Hydraulic Engineering 144 (6) (2018) 04018030.
[10] X. Wang, J. Lin, A. Keramat, M.S. Ghidaoui, S. Meniconi, B. Brunone, Matched-field processing for leak localization in a viscoelastic pipe: An experimental study, Mechanical Systems and Signal Processing 124 (2019) 459–478.
[11] H.-F. Duan, Transient frequency response based leak detection in water supply pipeline systems with branched and looped junctions, Journal of Hydroinformatics 19 (1) (2016) 17–30.
[12] M. Ferrante, B. Brunone, S. Meniconi, Leak detection in branched pipe systems coupling wavelet analysis and a lagrangian model, Journal of Water Supply: Research and Technology-AQUA 58 (2) (2009) 95–106.
[13] S.B. Beck, M.D. Curren, N.D. Sims, R. Stanway, Pipeline network features and leak detection by cross-correlation analysis of reflected waves, Journal of Hydraulic Engineering 131 (8) (2005) 715–723.
[14] M.F. Ghazali, S.B.M. Beck, J.D. Shucksmith, J.B. Boxall, W.J. Staszewski, Comparative study of instantaneous frequency based methods for leak detection in pipeline networks, Mechanical Systems and Signal Processing 29 (2012) 187–200.
[15] Z.S. Kapelan, D.A. Savic, G.A. Walters, A hybrid inverse transient model for leakage detection and roughness calibration in pipe networks, Journal of Hydraulic Research 41 (5) (2003) 481–492.
[16] C. Capponi, M. Ferrante, A.C. Zecchin, J. Gong, Leak detection in a branched system by inverse transient analysis with the admittance matrix method, Water Resources Management 31 (13) (2017) 4075–4089.
[17] S. Kim, Impedance method for abnormality detection of a branched pipeline system, Water Resources Management 30 (3) (2016) 1101–1115.
[18] A.C. Zecchin, L.B. White, M.F. Lambert, A.R. Simpson, Parameter identification of fluid line networks by frequency-domain maximum likelihood estimation, Mechanical Systems and Signal Processing 37 (1–2) (2013) 370–387.
[19] X. Wang, G.A. Camino, T.-C. Che, M.S. Ghidaoui, Factorized wave propagation model in tree-type pipe networks and its application to leak localization, Mechanical Systems and Signal Processing 147 (2021), 107116.
[20] M.L. Stephens, M.F. Lambert, A.R. Simpson, Determining the internal wall condition of a water pipeline in the field using an inverse transient, Journal of Hydraulic Engineering 139 (3) (2012) 310–324.
[21] D. Covas, H. Ramos, Case studies of leak detection and location in water pipe systems by inverse transient analysis, Journal of Water Resources Planning and Management 136 (2) (2010) 248–257.
[22] J.D. Shucksmith, J.B. Boxall, W.J. Staszewski, A. Seth, S.B.M. Beck, Onsite leak location in a pipe network by cepstrum analysis of pressure transients, Journal-American Water Works Association 104 (8) (2012) E457–E465.
[23] A. Haghighi, D. Covas, H. Ramos, Direct backward transient analysis for leak detection in pressurized pipelines: from theory to real application, Journal of Water Supply: Research and Technology-Aqua 61 (3) (2012) 189–200.
[24] S. Meniconi, B. Brunone, M. Ferrante, C. Capponi, C.A. Carrettini, C. Chiesa, D. Segalini, E.A. Lanfranchi, Anomaly pre-localization in distribution–transmission mains by pump trip: preliminary field tests in the milan pipe system, Journal of Hydroinformatics 17 (3) (2015) 377–389.
[25] J. Gong, M.L. Stephens, N.S. Arbon, A.C. Zecchin, M.F. Lambert, A.R. Simpson, On-site non-invasive condition assessment for cement mortar–lined metallic pipelines by time-domain fluid transient analysis, Structural Health Monitoring 14 (5) (2015) 426–438.
[26] C. Zhang, A.C. Zecchin, M.F. Lambert, J. Gong, A.R. Simpson, Multi-stage parameter-constraining inverse transient analysis for pipeline condition assessment, Journal of Hydroinformatics 20 (2) (2018) 281–300.
[27] T.-H. Yi, H.-N. Li, M. Gu, A new method for optimal selection of sensor location on a high-rise building using simplified finite element model, Structural Engineering and Mechanics 37 (6) (2011) 671–684.
[28] T.-H. Yi, H.-N. Li, X.-D. Zhang, A modified monkey algorithm for optimal sensor placement in structural health monitoring, Smart Materials and Structures 21 (10) (2012), 105033.
[29] Z. Qi, F. Zheng, D. Guo, H.R. Maier, T. Zhang, T. Yu, Y. Shao, Better understanding of the capacity of pressure sensor systems to detect pipe burst within water distribution networks, Journal of Water Resources Planning and Management 144 (7) (2018), 04018035.
[30] Q. Zhang, F. Zheng, Z. Kapelan, D. Savic, G. He, Y. Ma, Assessing the global resilience of water quality sensor placement strategies within water distribution systems, Water Research 172 (2020), 115527.
[31] J.P. Vítkovskỳ, J.A. Liggett, A.R. Simpson, M.F. Lambert, Optimal measurement site locations for inverse transient analysis in pipe networks, Journal of Water Resources Planning and Management 129 (6) (2003) 480–492.
[32] H. Shamloo, A. Haghighi, Optimum leak detection and calibration of pipe networks by inverse transient analysis, Journal of Hydraulic Research 48 (3) (2010) 371–376.
[33] M.M. Gamboa-Medina, L.F.R. Reis, Sampling design for leak detection in water distribution networks, Procedia Engineering 186 (2017) 460–469.
[34] A.H. Ayati, M.H. Ranginkaman, A.E. Bakhshipour, A. Haghighi, Transient measurement site design in pipe networks using the decision table method (DTM), Journal of Hydraulic Structures 5 (2) (2019) 32–48.

[35] A. Keramat, X. Wang, M. Louati, S. Meniconi, B. Brunone, M.S. Ghidaoui, Objective functions for inverse transient analysis based pipeline leakage detection: least square and matched-filter, Journal of Water Resources Planning and Management 145 (10) (2019), 04019042.
[36] B. Porat, B. Friedlander, Analysis of the asymptotic relative efficiency of the MUSIC algorithm, IEEE Transactions on Acoustics, Speech, and Signal Processing 36 (4) (1988) 532–544.
[37] X. Wang, M.S. Ghidaoui, Identification of multiple leaks in pipeline: Linearized model, maximum likelihood, and super-resolution localization, Mechanical Systems and Signal Processing 107 (2018) 529–548.
[38] X. Wang, M.S. Ghidaoui, Identification of multiple leaks in pipeline II: Iterative beamforming and leak number estimation, Mechanical Systems and Signal Processing 119 (2019) 346–362.
[39] X. Wang, M.S. Ghidaoui, J. Lin, Identification of multiple leaks in pipeline III: Experimental results, Mechanical Systems and Signal Processing 130 (2019) 395–408.
[40] X. Wang, D.P. Palomar, L. Zhao, M.S. Ghidaoui, R.D. Murch, Spectral-based methods for pipeline leakage localization, Journal of Hydraulic Engineering 145 (3) (2019), 04018089.
[41] A. Keramat, M.S. Ghidaou, X. Wang, M. Louati, Cramer-rao lower bound for performance analysis of leak detection, Journal of Hydraulic Engineering 145 (6) (2019), 04019018.
[42] A. Keramat, R. Zanganeh, Statistical performance analysis of transient-based extended blockage detection in a water supply pipeline, Journal of Water Supply: Research and Technology-Aqua (2019).
[43] H. Gazzah, S. Marcos, Cramer-Rao bounds for antenna array design, IEEE Transactions on Signal Processing 54 (1) (2006) 336–345.
[44] H. Gazzah, K. Abed-Meraim, Optimum ambiguity-free directional and omnidirectional planar antenna arrays for DOA estimation, IEEE Transactions on Signal Processing 57 (10) (2009) 3942–3953.
[45] H. Gazzah, Optimum antenna arrays for isotropic direction finding, IEEE Transactions on Aerospace and Electronic Systems 47 (2) (2011) 1482–1489.
[46] H. Gazzah, J.P. Delmas, CRB-based design of linear antenna arrays for near-field source localization, IEEE Transactions on Antennas and Propagation 62 (4) (2014) 1965–1974.
[47] X. Wang, E. Aboutanios, M.G. Amin, Adaptive array thinning for enhanced DOA estimation, IEEE Signal Processing Letters 22 (7) (2014) 799–803.
[48] J.P. Delmas, M.N. El Korso, H. Gazzah, M. Castella, CRB analysis of planar antenna arrays for optimizing near-field source localization, Signal Processing 127 (2016) 117–134.
[49] S. Asmussen, P.W. Glynn, Stochastic Simulation: Algorithms and Analysis,, volume 57, Springer Science & Business Media, 2007.
[50] W.J. Morokoff, R.E. Caflisch, Quasi-monte carlo integration, Journal of Computational Physics 122 (2) (1995) 218–230.
[51] I.M. Sobol, On the distribution of points in a cube and the approximate evaluation of integrals, Zh. Vychisl. Mat. Mat. Fiz. 7 (4) (1967) 784–802.
[52] A. Dubey, Z. Li, P.J. Lee, R. Murch, Measurement and characterization of acoustic noise in water pipeline channels, IEEE Access 7 (2019) 56890–56903.
[53] O. Piller, D. Gilbert, Jakobus E. Van Z. Dual calibration for coupled flow and transport models of water distribution systems, in: Water Distribution Systems Analysis 2010, 2010, pp. 722–731..
[54] S. Chu, T. Zhang, Y. Shao, T. Yu, H. Yao, Numerical approach for water distribution system model calibration through incorporation of multiple stochastic prior distributions, Science of The Total Environment 708 (2020), 134565.
[55] X. Wang, M. Waqar, H.-C. Yan, M. Louati, M.S. Ghidaoui, P.J. Lee, S. Meniconi, B. Brunone, B. Karney, Pipeline leak localization using matched-field processing incorporating prior information of modeling error, Mechanical Systems and Signal Processing 143 (2020), 106849.
[56] E.T. Jaynes, Probability Theory: The Logic of Science, Cambridge University Press, 2003.
[57] P.J. Lee, H.-F. Duan, M. Ghidaoui, B. Karney, Frequency domain analysis of pipe fluid transient behaviour, Journal of Hydraulic Research 51 (6) (2013) 609–622.
[58] M.H. Chaudhry, Applied Hydraulic Transients, third ed., Springer, 2014.
[59] X. Wang, M.S. Ghidaoui, P.J. Lee, Linear model and regularization for transient wave-based pipeline-condition assessment, Journal of Water Resources Planning and Management 146 (5) (2020), 04020028.
[60] P.J. Lee, J.P. Vítkovskỳ, Quantifying linearization error when modeling fluid pipeline transients using the frequency response method, Journal of Hydraulic Engineering 136 (10) (2010) 831–836.
[61] X. Wang, J. Lin, M.S. Ghidaoui, Usage and effect of multiple transient tests for pipeline leak detection, Journal of Water Resources Planning and Management 146 (11) (2020) 06020011.